J. Fluid Mech. (1992), *vol.* 241, *pp.* 403–419
Printed in Great Britain

The effect of axial stretching on the three-dimensional stability of a vortex pair

By J. S. MARSHALL
Department of Ocean Engineering, Florida Atlantic University, Boca Raton, FL 33431, USA

(Received 17 April 1991 and in revised form 26 December 1991)

The stability of a pair of counter-rotating vortices to three-dimensional disturbances in the presence of a stretching flow is studied for vortices of small circular cross-section. The problem is reduced to a system of two first-order, linear ordinary differential equations, which can be integrated numerically to obtain the change in the perturbation of the vortex pair with time. The stability of the vortex pair depends upon four dimensionless constants, two of which characterize the stretching flow. Computations indicate that stretching usually exerts a stabilizing influence on the vortex pair, although in many cases the perturbation amplitude may initially increase and then decrease at some later time due to the effects of stretching. The results of the study are applied to investigate stability of hairpin vortices that are typically observed in turbulent shear flows. An estimate of the percentage increase in perturbation amplitude of a hairpin vortex in a homogeneous turbulent shear flow is given as a function of the stretch of the hairpin for different values of the dimensionless perturbation wavenumber and the microscale Reynolds number $Re_\lambda = \lambda q/\nu$ (based on the Taylor microscale λ and the turbulent kinetic energy $\frac{1}{2}q^2$). The maximum percentage growth of a perturbation of the legs of a hairpin vortex in a turbulent shear flow is found to decrease with increase in Re_λ.

1. Introduction

A well-known paper by Crow (1970) shows that a pair of parallel counter-rotating vortices may become unstable to small three-dimensional disturbances under certain circumstances, whereas a single vortex in an otherwise stationary and unbounded domain is marginally stable to small disturbances (in the absence of axial flow). In the same paper, Crow introduced an approximate method for calculation of the motion of vortex filaments in which the 'external' flow is obtained using the Biot–Savart integral (with a 'cutoff' to remove the singularity in this integral for points on a vortex filament), and then assumes that the vortices are convected with the external flow field. Moore (1972) utilized a similar cutoff procedure (due to Rosenhead, 1930) to numerically compute the unstable vortex motion when the wave amplitude is not small, and these computations indicate that Crow's results (for small perturbations) hold remarkably well nearly up to the point at which the two vortices touch. Crow's problem was further extended by Robinson & Saffman (1982), who consider the three-dimensional linear stability of various vortex arrays, including a single row of vortices, a Kármán vortex street and a symmetric double row of vortices.

The effect of axial flow within the vortex cores on three-dimensional stability of a vortex pair was considered by Moore & Saffman (1972) and Widnall & Bliss (1971).

In this case, the simple assumption that a vortex is convected with the 'exterior' flow is not sufficient because of the effect of centrifugal forces caused by the axial flow in a curved vortex core. A new model for computation of vortex motion was introduced in these two papers, in which each element of the vortex core is endowed with some momentum and the rate of change of momentum of a vortex element is equated to the sum of external forces acting on the core lateral surface and internal contact forces. The external forces are related to Kutta–Joukowski lift and inertial drag (added mass and buoyancy forces) when the core radius is uniform along the axis. The external flow field is used in determining external forces on the core and is again calculated using the Biot–Savart integral with a cutoff. This approach for calculating vortex motion was extended by Lundgren & Ashurst (1989) and Marshall (1991) to study problems with variable core area. The latter study utilized a 'directed curve' model to represent the vortex core (which is found to be a useful approach for modelling nonlinear variations in core area); however, the final equations can be reduced in appropriate limits to those of the previously cited vortex theories.

Many cases involving vortex pairs in nature do not involve vortices that are immersed in an otherwise quiescent medium (as assumed in the previously cited articles on the Crow instability), but instead involve vortices which are subject to stretching along their axes. A notable example of this observation is the hairpin vortices found in turbulent shear flows, which are believed to exert a strong influence on Reynolds stress and turbulence production rates. Other vortices found in turbulent flows, such as streamwise or transverse vortices, may also undergo stretching when the mean velocity has a non-zero gradient. Examples of vortex pairs undergoing stretching are also plentiful for larger-scale vortices, as exemplified by an oceanic vortex pair travelling from shallow to deep water or by airfoil trailing vortices in the near wake of an aircraft.

The present paper is composed of two parts. The first part (§2) addresses the problem of the three-dimensional linear stability of a counter-rotating vortex pair in a stretching flow. The problem is reduced to a system of first-order ordinary differential equations, which are then solved numerically to determine the change in perturbation amplitude with time. In the second part (§3), the results of §2 are applied to study the instability of hairpin vortices typical of those observed in turbulent shear flows. An argument is made in this section that the instability and subsequent break-up of hairpin vortices (at least in homogeneous shear flows) is due to the Crow instability between the hairpin legs. An estimate of the amplitude of perturbations along the hairpin legs is obtained as a function of the stretch of the hairpin vortex for different values of the microscale Reynolds number Re_λ in a homogeneous turbulent shear flow. The conclusions of the study are summarized in §4.

2. Stability analysis

We consider the stability of two parallel, infinitely long vortices in a stretching flow. The vortices are labelled vortex 1 and vortex 2, as shown in figure 1, and have axes C_1 and C_2 and circulations $\Gamma_1 = -\Gamma_0$ and $\Gamma_2 = \Gamma_0$. The separation distance between the vortices in the unperturbed flow is $b(t)$ and the vortex core radius is $\sigma_0(t)$. Throughout this section, it is assumed that the flow is inviscid and incompressible and that the ratio σ_0/b is very small compared to unity.

To calculate the vortex motion in a perturbed state, it is assumed that every point on each vortex at every time t is convected both by the induced velocity, which arises

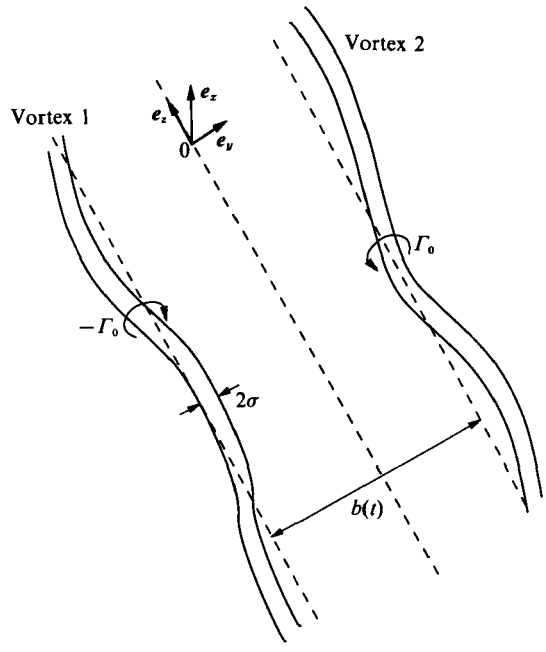

FIGURE 1. Sketch of a counter-rotating vortex pair with axes initially aligned in the z-direction. The separation distance between the unperturbed vortices is b and the circulation of the vortices is $\pm\Gamma_0$.

from the vortex itself and from the other vortex of the pair, and by some other prescribed velocity due to the stretching flow. Let $\boldsymbol{r}_N(\xi_N, t)$ denote the position vector from a fixed coordinate frame to a point on the axis C_N of vortex N, where ξ_N is a convected coordinate which measures arclength along C_N in some reference state. The velocity $\boldsymbol{v}_N(\xi_N, t)$ of vortex N is defined by

$$\boldsymbol{v}_N = \frac{\mathrm{d}\boldsymbol{r}_N}{\mathrm{d}t}, \tag{1}$$

where $\mathrm{d}/\mathrm{d}t$ denotes the material derivative, or the derivative with respect to time keeping ξ_N fixed. If $\boldsymbol{u}_N(\xi_N, t)$ denotes the sum of the self-induced velocity and the velocity induced by the opposing vortex and $\boldsymbol{w}_N(\xi_N, t)$ denotes some other prescribed flow, then the vortex motion is obtained from the equation

$$\boldsymbol{v}_N = \boldsymbol{u}_N + \boldsymbol{w}_N, \tag{2}$$

where $\boldsymbol{u}_N$ is given by the Biot–Savart integral as

$$\boldsymbol{u}_N = \sum_{M=1}^{2} -\frac{\Gamma_M}{4\pi} \int_{-\infty}^{\infty}_{[\delta_c]} \frac{[\boldsymbol{r}_N(\xi_N, t) - \boldsymbol{r}_M(\xi'_M, t)]}{|\boldsymbol{r}_N(\xi_N, t) - \boldsymbol{r}_M(\xi'_M, t)|^3} \mathrm{d}\boldsymbol{r}_M(\xi'_M, t). \tag{3}$$

A prime in (3) denotes a dummy variable of integration. Also, $[\delta_c]$ placed under the integral sign implies that a segment of length $\delta_c\,\sigma(\xi_N, t)$ will be cut out of the domain of integration each side of ξ_N when $M = N$, where following Crow (1970) and assuming uniform vorticity in the core, we take

$$\delta_c = \tfrac{1}{2}\exp(\tfrac{1}{4}) \approx 0.6420. \tag{4}$$

Note that the approximate system of equations (2)–(3) is the same as that used by Crow (1970) and a number of other workers, and (2) can be derived from more general equations governing vortex motion (see Moore & Saffman 1972 or Marshall 1991) as a leading-order approximation for small values of the ratio σ/b.

Since the vortex axes are initially aligned in the z-direction, then

$$\boldsymbol{r}_N(\xi_N,t)-\boldsymbol{r}_M(\xi'_M,t) = (\xi_N-\xi'_M)\,\boldsymbol{e}_z+b(1-\delta_{NM})\,\boldsymbol{e}_y+\boldsymbol{p}_N(\xi_N,t)-\boldsymbol{p}_M(\xi'_M,t), \tag{5}$$

where δ_{NM} is the Kronecker delta and $\boldsymbol{p}_M$ is the perturbation of vortex M. We now identify $t=0$ as the reference state in which ξ_N measures arclength on C_N, and further let the perturbation of vortex N be initialized at $t=0$ and be given by

$$\boldsymbol{p}_N(\xi_N,t) = x_N\,\boldsymbol{e}_x+y_N\,\boldsymbol{e}_y+z_N\,\boldsymbol{e}_z. \tag{6}$$

In (6), x_N, y_N and z_N are functions of ξ_N and t.

The velocities $\boldsymbol{v}_N$, $\boldsymbol{u}_N$ and $\boldsymbol{w}_N$ in (2) are each composed of the sum of a part present in the unperturbed flow (denoted by a capital letter) and a perturbed part (denoted by a lower-case letter) and are written in component form as

$$\boldsymbol{v}_N = (v_{Ni}+V_{Ni})\,\boldsymbol{e}_i, \quad \boldsymbol{u}_{Ni} = (u_{Ni}+U_{Ni})\,\boldsymbol{e}_i, \quad \boldsymbol{w}_N = (w_{Ni}+W_{Ni})\,\boldsymbol{e}_i, \tag{7}$$

where $\boldsymbol{e}_i$ are Cartesian base vectors and summation over repeated tensor indices, having the values $i=(1,2,3)$, is implied. The unperturbed flow at $t=0$ is given by

$$\left.\begin{aligned} &U_{N1} = -\frac{\Gamma_0}{2\pi b}, \quad U_{N2} = U_{N3} = 0, \\ &W_{N1} = 0, \quad W_{N2} = \tfrac{1}{2}(-1)^N c_2 b, \quad W_{N3} = c_3 z, \\ &V_{Ni} = U_{Ni}+W_{Ni}, \end{aligned}\right\} \tag{8}$$

and the prescribed perturbation velocity components w_{Ni} (due to the stretching flow) are

$$w_{N1} = c_1 x_N, \quad w_{N2} = c_2 y_N, \quad w_{N3} = c_3 z_N. \tag{9}$$

In (8) and (9), c_3 is the stretching rate and to satisfy continuity we must have

$$c_1+c_2+c_3 = 0. \tag{10}$$

The vortex core radius σ is composed of the sum of a part $\sigma_0(t)$ in the unperturbed flow and a perturbed part $\sigma_p(\xi_N,t)$. To be consistent with (8), we let σ_0 and b vary with time as

$$\sigma_0(t) = \sigma_{\mathrm{I}}\exp(-\tfrac{1}{2}c_3 t), \quad b(t) = b_{\mathrm{I}}\exp(c_2 t), \tag{11}$$

where σ_{I} and b_{I} are constant initial values. The perturbation part of $\boldsymbol{v}_N$ in (7) is related to the perturbation displacement vector $\boldsymbol{p}_N$ in (6) by

$$v_{Ni} = \frac{\mathrm{d}p_{Ni}}{\mathrm{d}t}. \tag{12}$$

We consider only perturbations with small amplitude and small slope, or with

$$0 < \max\left|\frac{\boldsymbol{p}_N}{b}\right| \ll 1, \quad 0 < \max\left|\frac{\partial \boldsymbol{p}_N}{\partial \xi_N}\right| \ll 1. \tag{13}$$

We restrict attention to the case in which fluid particles on the vortex axis are perturbed only in the (x,y)-plane, so we set $z_N = 0$ and note that the linearized axial

component of (2) reduces to an identity in this case. The linearized equations for x_N and y_N are obtained from (2), (9) and (12) as

$$\frac{\partial x_N}{\partial t}+c_3 z\frac{\partial x_N}{\partial z}=u_{N1}+c_1 x_N, \tag{14}$$

$$\frac{\partial y_N}{\partial t}+c_3 z\frac{\partial y_N}{\partial z}=u_{N2}+c_2 y_N, \tag{15}$$

where x_N and y_N are functions of time t and the coordinate z in the $\boldsymbol{e}_z$ direction (which should not be confused with the axial perturbation z_N of the vortex). Note that the perturbation σ_p in core radius does not enter into the linearized equations for x_N and y_N.

A solution of the linear integro-differential system (3) and (15) is assumed to exist of the form

$$x_N=\hat{x}_N(t)\,\mathrm{e}^{\mathrm{i}zk(t)},\quad y_N=\hat{y}_N(t)\,\mathrm{e}^{\mathrm{i}zk(t)}, \tag{16}$$

where the wavenumber k of the perturbation is some function of time whose form is to be determined. For solutions of the form (16), it was shown by Crow (1970) that the Biot–Savart integral (3) can be reduced to

$$\left.\begin{aligned}
u_{11}&=(\Gamma_0/2\pi b^2)[-y_1+\chi(kb)\,y_2+(kb)^2\omega(\delta_c\,k\sigma_0)\,y_1],\\
u_{12}&=(\Gamma_0/2\pi b^2)[-x_1+\psi(kb)\,x_2-(kb)^2\omega(\delta_c\,k\sigma_0)\,x_1],\\
u_{21}&=(\Gamma_0/2\pi b^2)[y_2-\chi(kb)\,y_1-(kb)^2\omega(\delta_c\,k\sigma_0)\,y_2],\\
u_{22}&=(\Gamma_0/2\pi b^2)[x_2-\psi(kb)\,x_1+(kb)^2\omega(\delta_c\,k\sigma_0)\,x_2].
\end{aligned}\right\} \tag{17}$$

The first index attached to u in (17) designates the vortex number N and the second index is the component number i. The functions x_N and y_N in (17) are again functions of both z and t, and the expressions (17) will only be valid when a solution for x_N and y_N can be found of the form (16). Defining $\delta=\delta_c\,k\sigma_0$ and $\beta=kb$, the 'self-induction' function $\omega(\delta)$ and 'mutual-induction' functions $\chi(\beta)$ and $\psi(\beta)$ are defined in terms of the modified Bessel functions of the second kind, K_0 and K_1, and the cosine integral, $\mathrm{Ci}\,(\delta)$, as

$$\left.\begin{aligned}
\omega(\delta)&=\tfrac{1}{2}\{[\cos(\delta)-1]/\delta^2+\sin(\delta)/\delta-\mathrm{Ci}\,(\delta)\},\\
\psi(\beta)&=\beta^2K_0(\beta)+\beta K_1(\beta),\quad \chi(\beta)=\beta K_1(\beta).
\end{aligned}\right\} \tag{18}$$

Dimensionless normal modes, designated as 'symmetric' and 'antisymmetric', are defined by

$$x_S=\frac{x_2+x_1}{b_I},\quad y_S=\frac{y_2-y_1}{b_I},\quad x_A=\frac{x_2-x_1}{b_I},\quad y_A=\frac{y_2+y_1}{b_I}. \tag{19}$$

A dimensionless time τ and dimensionless axial distance ζ are defined by

$$\tau=(\Gamma_0/b_I^2)\,t,\quad \zeta=(b_I c_3/\Gamma_0)\,z. \tag{20}$$

Various other dimensionless parameters ϵ, F_1, F_2, G_1 and G_2 are also introduced as follows:

$$\left.\begin{aligned}
\epsilon&=\frac{b_I^2 c_3}{\Gamma_0},\quad F_1=\frac{1}{2\pi}[1+\chi(\beta)-\beta^2\omega(\delta)],\quad F_2=\frac{1}{2\pi}[1-\psi(\beta)+\beta^2\omega(\delta)],\\
G_1&=\frac{1}{2\pi}[1-\chi(\beta)-\beta^2\omega(\delta)],\quad G_2=\frac{1}{2\pi}[1+\psi(\beta)+\beta^2\omega(\delta)].
\end{aligned}\right\} \tag{21}$$

Using (14)–(15) and (17)–(21), the dimensionless perturbation equations for the two normal modes become

$$\frac{\partial \boldsymbol{x}_S}{\partial \tau}+\epsilon\zeta\frac{\partial \boldsymbol{x}_S}{\partial \zeta}=\boldsymbol{A}_S(\tau)\,\boldsymbol{x}_S, \qquad \frac{\partial \boldsymbol{x}_A}{\partial \tau}+\epsilon\zeta\frac{\partial \boldsymbol{x}_A}{\partial \zeta}=\boldsymbol{A}_A(\tau)\,\boldsymbol{x}_A, \tag{22a, b}$$

where

$$\boldsymbol{x}_S=\begin{bmatrix}x_S\\ y_S\end{bmatrix}, \quad \boldsymbol{x}_A=\begin{bmatrix}x_A\\ y_A\end{bmatrix}, \quad \boldsymbol{A}_S=\begin{bmatrix}\epsilon c_1/c_3 & F_1\\ F_2 & \epsilon c_2/c_3\end{bmatrix}, \quad \boldsymbol{A}_A=\begin{bmatrix}\epsilon c_1/c_3 & G_1\\ G_2 & \epsilon c_2/c_3\end{bmatrix}. \tag{22c}$$

It is noted that since σ_0, b, k all depend on time, then δ, β and consequently F_1, F_2, G_1 and G_2 also depend on time. Equations (22a, b) can be solved using the method of characteristics. The characteristic lines $\zeta=\zeta(\tau)$ are given by

$$\zeta=\zeta_0\,\mathrm{e}^{\epsilon\tau}, \tag{23}$$

where ζ_0 is an initial position of the characteristic at $\tau=0$. Using (23), equations (22a, b) for $\boldsymbol{x}_S$ and $\boldsymbol{x}_A$ then reduce to the ordinary differential equations

$$\frac{\mathrm{d}\boldsymbol{x}_S}{\mathrm{d}t}=\boldsymbol{A}_S(\tau)\,\boldsymbol{x}_S, \quad \frac{\mathrm{d}\boldsymbol{x}_A}{\mathrm{d}t}=\boldsymbol{A}_A(\tau)\,\boldsymbol{x}_A. \tag{24a, b}$$

The solution to (24) for $\boldsymbol{x}_S$ will be of the form

$$\boldsymbol{x}_S=\begin{bmatrix}B_1(\zeta_0)f_1(\tau)\\ B_2(\zeta_0)f_2(\tau)\end{bmatrix}, \tag{25}$$

and similarly for $\boldsymbol{x}_A$. The coefficients B_1 and B_2 are arbitrary functions of ζ_0, whose form is determined by initial conditions at $\tau=0$. If we choose initial conditions such that

$$B_1(\zeta_0)=\bar{B}_1\exp(\mathrm{i}\zeta_0), \tag{26}$$

where $\bar{B}_1$ is independent of ζ_0 (with similar forms for B_2 and the coefficients of $\boldsymbol{x}_A$), then using (23) it follows that the solutions for x_N and y_N are of the form (16), with the wavenumber $k(t)$ given in terms of dimensional variables by

$$k(t)=k_0\exp(-c_3 t). \tag{27}$$

From (11) and (17), the parameters β and δ are found to vary with dimensionless time τ as

$$\delta(\tau)=\delta_0\exp(-\tfrac{3}{2}\epsilon\tau), \quad \beta(\tau)=\beta_0\exp[-(1-c_2/c_3)\,\epsilon\tau]. \tag{28}$$

Substituting (28) into (18) to calculate $\omega(\delta)$, $\psi(\beta)$ and $\chi(\beta)$, we can determine the variation of $\boldsymbol{A}_S$ and $\boldsymbol{A}_A$ with τ from (21) and (22c). For any initial condition of the form (25)–(26), the problem reduces to solution of (24) for known $\boldsymbol{A}_S$ and $\boldsymbol{A}_A$, which can be obtained numerically using any standard forward-marching method. Solution of these equations depends upon the four dimensionless constants ϵ, δ_0, β_0 and c_1/c_3. One might imagine, therefore, that the stability domain for the vortex pair can be represented as a region in the four-dimensional space of these parameters. In practice, however, determination of a discrete stability domain of this type is difficult because many instances have been found in which the perturbation amplitude initially increases and then decreases at a later time and eventually approaches zero. In some such cases (which might be considered unstable), the perturbation amplitude may reach a value of order unity before the maximum is reached, at which point the linearized analysis would no longer be valid and touching of the opposing vortices

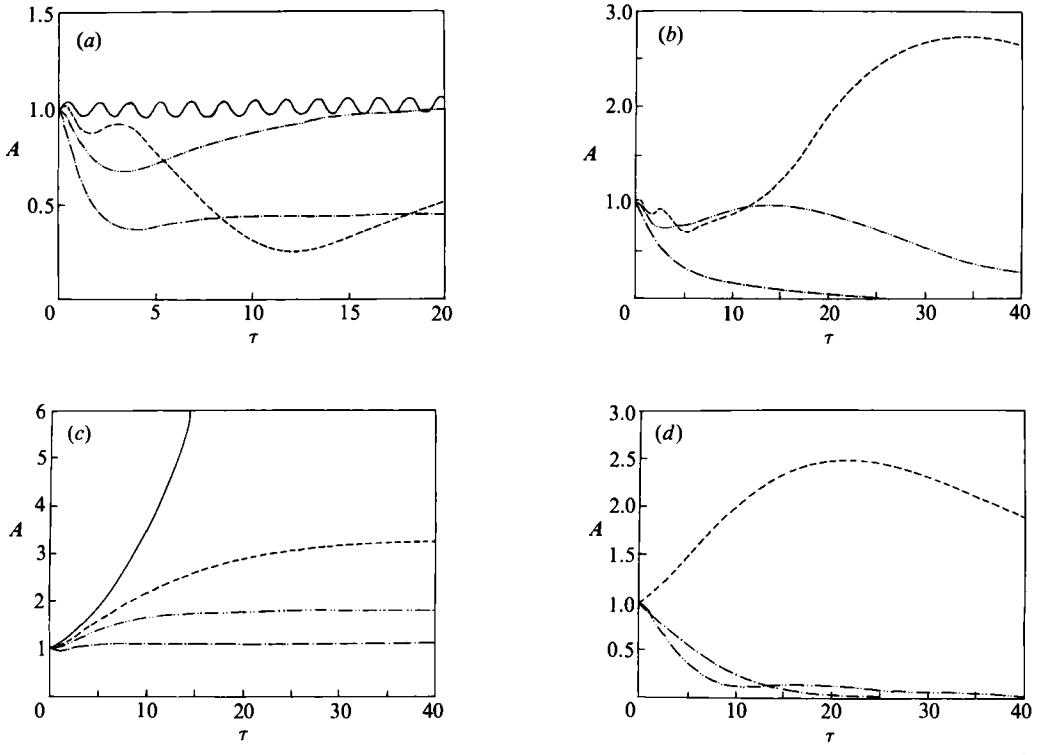

FIGURE 2. Sample calculations showing the change in perturbation amplitude ratio A with dimensionless time τ in the symmetric mode for values of stretching parameter ϵ of 0 (——), 0.1 (– – – –), 0.2 (— ·· — ·· — ·· —) and 0.5 (— · — · —). (a, b) $\delta_0 = 0.2$ and $\beta_0 = 4$ (which is stable for $\epsilon = 0$); (c, d) $\delta_0 = 0.3$ and $\beta_0 = 1$ (which is unstable for $\epsilon = 0$). The ratio c_1/c_3 is 0 in (a, c) and $-\frac{1}{2}$ in (b, d).

may well occur. In other such cases (which might be considered stable), the maximum perturbation amplitude is well within the range of the linear theory and we find that no touching of the opposing vortices can occur.

Equations (24) are solved numerically using the fourth-order Runge–Kutta method for various values of the constants ϵ, c_1/c_3, δ_0 and β_0, and the results of some of these calculations are shown for the symmetric mode in figure 2(a–d) and for the antisymmetric mode in figure 3(a–d). In these figures, the 'amplitude ratio' A is plotted against dimensionless time τ, where A is defined for the symmetric mode by

$$A = [x_s^2(\tau) + y_s^2(\tau)]^{\frac{1}{2}} / [x_s^2(0) + y_s^2(0)]^{\frac{1}{2}}, \tag{29}$$

and similarly for the antisymmetric mode. The value of $A(\tau)$ thus represents the ratio of the perturbation amplitude at time τ to the initial perturbation amplitude at $\tau = 0$. For all curves in figures 2 and 3, we set $x_s(0) = y_s(0)$ or $x_A(0) = y_A(0)$, although the results did not qualitatively differ for other choices of the initial values.

Figures 2(a) and 3(a) show the effect of the stretching parameter ϵ on flows which are steady in the absence of stretching (for which $\epsilon = 0$) with $c_1/c_3 = 0$. The $\epsilon = 0$ results for A oscillate with τ at a constant amplitude, and the results for $\epsilon > 0$ also exhibit values of A near unity which approach some constant value as $\tau \to \infty$. The cases in figures 2(a) and 3(a) are shown again in figures 2(b) and 3(b), respectively, but now with $c_1/c_3 = c_2/c_3 = -\frac{1}{2}$. In all cases for which $\epsilon > 0$, the amplitude ratio either decays immediately to zero, or else attains some maximum value at a finite τ

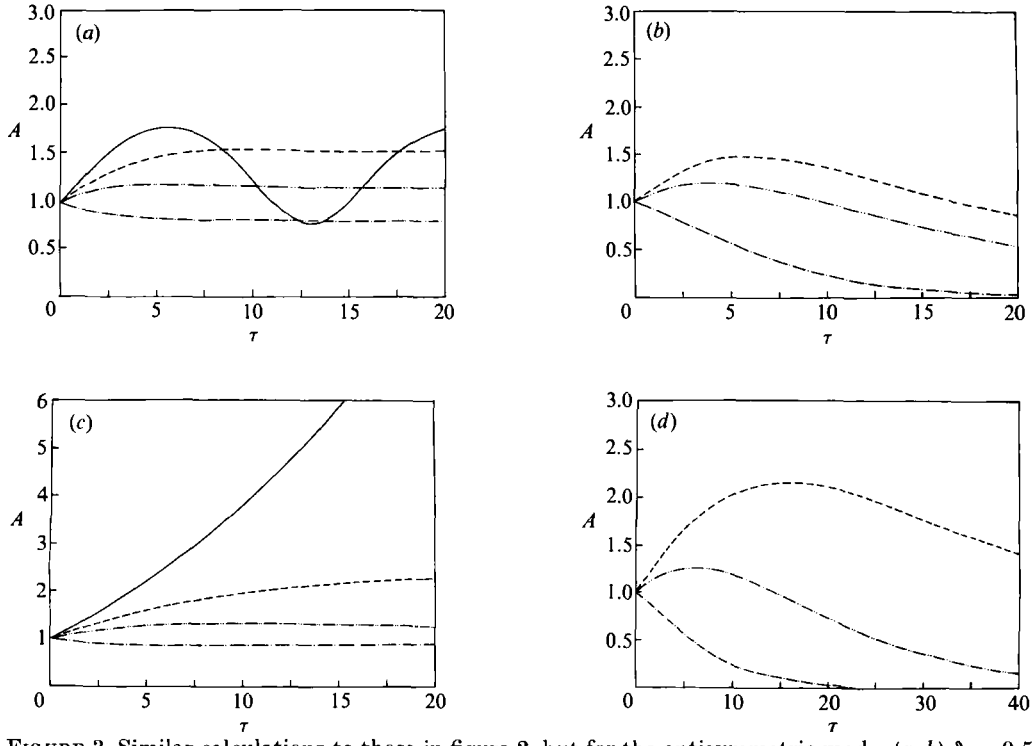

FIGURE 3. Similar calculations to those in figure 2, but for the antisymmetric mode. (a, b) $\delta_0 = 0.5$ and $\beta_0 = 2$ (which is stable for $\epsilon = 0$); (c, d) $\delta_0 = 0.5$ and $\beta_0 = 1$ (which is unstable for $\epsilon = 0$). Values of ϵ for the different type lines in (a–d) are the same as in figure 2 (a–d). The ratio c_1/c_3 is 0 in (a, c) and $-\frac{1}{2}$ in (b, d).

and then decays to zero. In some of these cases, however, the maximum value of A is fairly large (e.g. $A_{\max} \approx 2.7$ for $\epsilon = 0.1$ in figure 2b). In figures 2(c) and 3(c), cases are shown for $c_1/c_3 = 0$ which are unstable in the absence of stretching. Although for $\epsilon = 0$, $A \to \infty$ as $\tau \to \infty$ in the linearized analysis. It is found that for $\epsilon > 0$, A always approaches some finite asymptotic value as $\tau \to \infty$. This asymptotic value of A depends on ϵ and may be quite large for small ϵ. The cases shown in figures 2(c) and 3(c) are shown again in figures 2(d) and 3(d), respectively, but now with $c_1/c_3 = -\frac{1}{2}$. We find again that the values of A either reach a maximum at some finite τ and then decrease to zero or else A decreases to zero immediately.

The results clearly indicate that vortex stretching exerts a strong stabilizing influence on the vortex pair instability. In fact, it can be shown from (22c) and (24) that the amplitude ratio A is always bounded as $\tau \to \infty$ for any $\epsilon > 0$ and c_1/c_3 in the interval $-1 \leqslant c_1/c_3 \leqslant 0$. This is not to say, however, that A may not become quite large at particular values of τ for certain $\epsilon > 0$, such that depending on the initial perturbation amplitude, the assumption (13) of small perturbations might be violated. It is found in all computations that A approaches some constant value as $\tau \to \infty$ for $c_1/c_3 = 0$ or -1, but that for $0 > c_1/c_3 > -1$, the value of A decreases to zero as $\tau \to \infty$ (sometimes preceded by a local maximum of A). We see from (24a) that $\mathrm{d}x_s/\mathrm{d}t$ may equal zero for non-zero x_s only when $\det(\boldsymbol{A}_s)$ vanishes, and similarly for the antisymmetric mode in (24b). For the symmetric mode, the determinant of $\boldsymbol{A}_s$ vanishes for any τ such that β and δ, determined from (28), satisfy the equation

$$F_1 F_2 = \epsilon^2 |(c_1/c_3)(1 + c_1/c_3)|. \tag{30}$$

For $c_1/c_3 = 0$ or -1, the right-hand side of (30) is zero. Since $F_1 \to 1/\pi$ and $F_2 \to 0$ as $\tau \to \infty$ from (18), (21) and (28), then (30) is always satisfied at infinite time, although it may be satisfied at other finite times as well.

The long-time behaviour of the perturbations can be obtained from (24) in the limit as $\tau \to \infty$, which yields the system of equations

$$\frac{\mathrm{d}x_s}{\mathrm{d}t} = \epsilon\bar{c}x_s + \frac{1}{\pi}y_s, \quad \frac{\mathrm{d}y_s}{\mathrm{d}t} = -\epsilon(1+\bar{c})\,y_s, \tag{31}$$

where $\bar{c} = c_1/c_3$ lies in the interval $-1 \leqslant \bar{c} \leqslant 0$. For $\bar{c}$ not equal to either -1 or 0, the solution of (31) gives x_s and y_s decreasing exponentially in time to zero. For either $\bar{c} = 0$ or -1, it is found that x_s and y_s approach constants as $\tau \to \infty$. The equations for the perturbations x_A and y_A become identical to (31) as $\tau \to \infty$, so the above conclusions hold for the antisymmetric mode as well.

3. Stability of hairpin vortices in turbulent shear flows

Hairpin vortices are known to be a dominant feature of many turbulent shear flows. The role and characteristics of these structures in turbulent flow is especially well documented by recent direct numerical simulations of turbulent channel flow and homogeneous shear flow (see Moin & Kim 1985, and Rogers & Moin 1987, who also cite previous experimental work). A primary observed feature of turbulent hairpin vortices is that they align themselves at some nearly constant angle to the mean flow direction (often around 45°) and allow themselves to be stretched by the mean flow. The work performed by the mean flow during stretching of hairpin vortices is a major source of turbulent energy production.

In this section, a model for hairpin vortices in homogeneous turbulent shear flows is presented and used to examine the instability of the hairpin structure. Two distinct instability mechanisms are considered for break-up of hairpins: (i) the three-dimensional Crow instability of a vortex pair (discussed in §2) and (ii) the essentially two-dimensional instability of Moore & Saffman (1971) for a vortex with elliptical cross-section which is subjected to a straining flow in the plane of vortex circulation. For this latter instability, the straining flow acting on one hairpin leg results from the flow field generated by the opposing hairpin leg. Extensions of this instability mechanism have been made by Kida (1981) for arbitrary core aspect ratio and strain rate and by Neu (1984) in the presence of axial stretching. Calculations by Moore & Saffman (1975*a*) (see also Pierrehumbert & Widnall 1981) indicate that a vortex pair will not become unstable under this mechanism until the cores of the vortices are nearly touching. After some consideration, it is argued in this section that the Moore–Saffman mechanism cannot play a role in the initial instability of hairpin vortices. Calculations using the result (24) of §2, on the other hand, yield very plausible predictions for growth of perturbations on hairpin legs based on the Crow mechanism. The effect of core deformation under a straining field on three-dimensional stability (as discussed by Moore & Saffman 1975*b*; Robinson & Saffman 1984 in the absence of axial stretching) is not considered in the present paper.

We consider a hairpin vortex (for which the leg separation distance b is much less than the length L) aligned at some angle θ to the direction of a homogeneous mean shear flow $\bar{\boldsymbol{w}}$ (see figure 4*a*), where for a constant shearing rate S,

$$\bar{\boldsymbol{w}} = Sy\boldsymbol{e}_x. \tag{32}$$

Let $\boldsymbol{s}$ be a unit direction tangent to the axes of the vortex legs (which are taken to

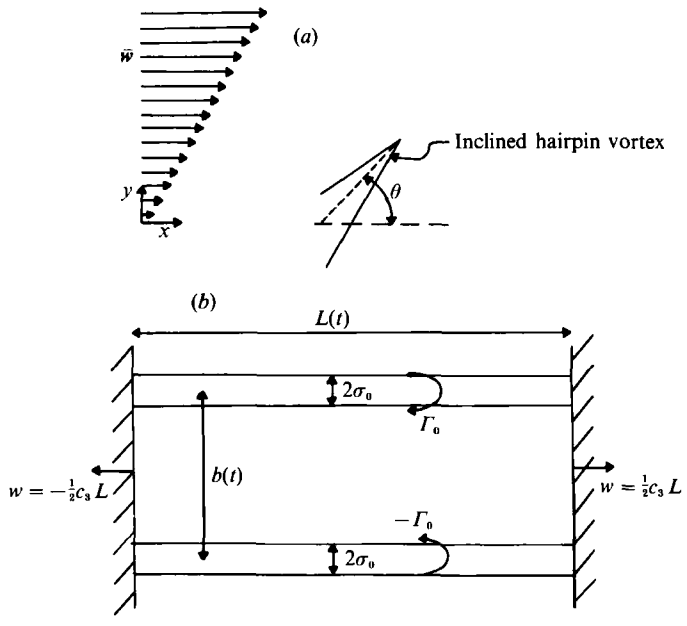

FIGURE 4. (*a*) Schematic of the legs of a hairpin vortex aligned at 45° to a mean shear flow. (*b*) Idealized model of the legs of a hairpin vortex for purposes of estimating the growth of three-dimensional perturbations of the hairpin legs.

be nearly parallel) and let $\boldsymbol{n}$ be an outward unit normal to the plane on which the hairpin vortex lies. Then $\bar{\boldsymbol{w}}$ can be written as

$$\bar{\boldsymbol{w}} = w_n \boldsymbol{n} + w_s \boldsymbol{s}, \tag{33}$$

where w_n and w_s are the components of $\bar{\boldsymbol{w}}$ in the $\boldsymbol{n}$- and $\boldsymbol{s}$-directions. If θ is the angle between the vortex axes and the x-axis, then from (32) and (33), we have

$$w_n = Sy \sin(\theta), \quad w_s = Sy \cos(\theta). \tag{34}$$

At a height y, the induced velocity $\boldsymbol{w}_1$ on a hairpin leg from the opposing leg (in the absence of perturbations of the legs) is approximately

$$\boldsymbol{w}_1 = -w_1 \boldsymbol{n} = -\frac{\Gamma_0}{2\pi b} \boldsymbol{n}, \tag{35}$$

where $b = b(y)$. The estimate (35) is not valid near the hairpin base ($y = 0$) or tip ($y = L/\sqrt{2}$).

The condition for the angle of inclination θ of the hairpin to be constant in time is that a reference frame translating with the vortex (but not rotating) exists in which the hairpin appears to undergo a purely stretching motion. It follows that the velocity of a point P on the hairpin axis can be decomposed into a uniform translation W in the x-direction and a stretching velocity w^* parallel to $\boldsymbol{\sigma}$, such that

$$\bar{\boldsymbol{w}} + \boldsymbol{w}_1 = w^* \boldsymbol{s} + W \boldsymbol{e}_x. \tag{36}$$

Taking the scalar product of (36) with $\boldsymbol{n}$ and then again with $\boldsymbol{s}$ and using (32)–(35), we obtain

$$Sy \sin(\theta) - \frac{\Gamma_0}{2\pi b} = W \sin(\theta), \qquad Sy \cos(\theta) - w^* = W \cos(\theta). \tag{37a, b}$$

Note that the vortex translation speed W will always be less than the mean flow rate Sy at any y along the hairpin axis becausc the induced velocity from the opposite leg of the hairpin has a component which opposes the mcan flow. There are three unknowns in (37): b and w^*, which depend on y, and W, which is a constant and is set by an initial condition on b. We now set $W = Sy_0$, where y_0 is some value of y slightly below the hairpin base. Solving (37) for leg separation length b and stretching rate w^* gives

$$b = \frac{\Gamma_0}{2\pi S(y-y_0)\sin(\theta)} \tag{38}$$

and

$$w^* = S(y-y_0)\cos(\theta). \tag{39}$$

Since the right-hand side of (38) is independent of time, we conclude that b must also be independent of time as the hairpin is stretched. Of course, this argument considers only induced velocity due to the legs of the hairpin and may not apply in the initial stages of hairpin growth. Evaluating (39) at $y-y_0 \approx L/\sqrt{2}$, where we assume that the hairpin is sufficiently stretched that the difference between y_0 and the location of the hairpin base is small compared to the hairpin length L, we can write

$$w^*(y = L/\sqrt{2}) = \frac{\mathrm{d}L}{\mathrm{d}t} = \tfrac{1}{2}\sqrt{2}SL\cos(\theta). \tag{40}$$

Integrating (38) gives the variation of hairpin length with time as

$$L(t) = L_1 \exp[\tfrac{1}{2}\sqrt{2}St\cos(\theta)], \tag{41}$$

where L_1 is the initial value of L.

We now consider a rather simplified idealization of the legs of a hairpin vortex shown in figure 4(*b*), which is expected to be valid away from the base and tip regions. The idealization consists of a pair of nearly parallel vortices that are separated by a distance b (prior to perturbation of the vortices) and have circulations $\pm\Gamma_0$ and core radii σ_0. The vortices are confined between two parallel plates (placed normal to the vortex axes) that are separated by a distance $L(t)$ and are pulled apart at a rate c_3. The values of L, b and σ_0 in the model are respectively identified with the length, median leg separation distance and core radius of a typical hairpin vortex in a turbulent shear flow. It is assumed that any perturbation in vortex separation distance must vanish at the plates (i.e. at $z = \pm\frac{1}{2}L$ in figure 4*b*), so that the perturbation wavenumber k is confined to the interval $k_{\min} \leqslant k < \infty$, where $k_{\min}(t) = \pi/L(t)$. This model is constructed to be the simplest possible that allows analysis of instability of the hairpin legs. In particular, the model neglects variation of leg separation distance with height, which is probably reasonable for short-wavelength disturbances but questionable for disturbances with wavelength on the order of the hairpin length. The following analysis based on this model is intended only to demonstrate that the Crow instability is a viable mechanism leading to break-up of hairpin vortices in turbulent flows and that axial stretching exerts a strong effect on the instability for problems of this type.

The four dimensionless parameters which control the stability of the vortex pair (ϵ, β, δ and c_1/c_3 in the notation of §2) are given for the model shown in figure 4(*b*) by

$$c_1/c_3 = -1, \quad \beta = bk_0\exp(-c_3t), \quad \epsilon = b^2c_3/\Gamma_0, \quad \delta = \delta_c\sigma_1 k_0\exp(-\tfrac{3}{2}c_3t). \tag{42a-d}$$

The result (42*a*) follows from (10) and the observation made following (39) that b

must be constant in time, which implies from (11) that $c_2 = 0$. From (41), we conclude that the stretching rate c_3 is given by

$$c_3 = \tfrac{1}{2}\sqrt{2S}\cos(\theta). \tag{43}$$

Also, (41)–(43) imply that β must have a minimum value $\beta_{\min}$ given by

$$\beta_{\min} = (\pi b/L_1)\exp(-c_3 t). \tag{44}$$

Before calculations for hairpin vortex stability can be made, it is necessary to obtain estimates for the constants b, L_1, σ_1 and Γ_0 that are appropriate for turbulent shear flows. In this effort, attention is focused on homogeneous shear flows (in the mean) with microscale Reynolds numbers Re_λ between about 20 and 400, and the estimates which are formulated here are based largely on data from the numerical simulation of Rogers & Moin (1987, hereafter referred to as RM), with some extrapolation to higher values of Re_λ. The various arguments used to develop this scaling are numbered for convenience.

(i) The equilibrium Burgers (1948) vortex solution is used to motivate a form for the initial core radius of the hairpin vortex as

$$\sigma_1 = A_1(\nu/S)^{\frac{1}{2}}. \tag{45}$$

From the data of RM, the constant A_1 is estimated to have a value between about 5 and 10.

(ii) An empirical result (RM, figure 23*a*), which has been demonstrated in numerical simulations for Re_λ between about 20 and 150, gives the ratio of the typical leg separation distance b to the mixing length $L_M = q^3/\epsilon_D$ (where $\frac{1}{2}q^2$ is the turbulent kinetic energy and ϵ_D is the rate of turbulent dissipation per unit mass) as

$$\frac{b}{L_M} = \left(\frac{10}{Re_\lambda}\right)^{\frac{4}{5}}. \tag{46}$$

We recall that b is constant throughout the stretching of the hairpin vortex.

(iii) The ratio Sq^2/ϵ_D is found by RM to asymptotically approach a constant in homogeneous shear flows, the value of which seems to vary with Re_λ. From the available experimental and computational data (RM, table 1), it seems that $Sq^2/\epsilon_D \approx 1.1\,Re_\lambda^{\frac{2}{3}}$ gives approximately the observed values of this ratio for Re_λ in the range under consideration. Recalling the definitions $L_M = q^3/\epsilon_D$ and $Re_\lambda = q\lambda/\nu$, as well as the usual estimate $\epsilon_D \approx 5\nu q^2/\lambda^2$ for the turbulent dissipation rate, we find that L_M can be written as

$$L_M = 0.5(\nu/S)^{\frac{1}{2}}Re_\lambda^{\frac{6}{5}}. \tag{47}$$

Combining (46) and (47) gives an expression for b as

$$b = 3.2(\nu/S)^{\frac{1}{2}}Re_\lambda^{\frac{2}{5}}. \tag{48}$$

(iv) It is noted by RM (p. 55) that the ratio ω_{rms}/S, where ω_{rms} is the root-mean-square vorticity, scales like Re_λ divided by Sq^2/ϵ_D in homogeneous turbulent shear flows. From their data, the correlation seems to be approximately given by $\omega_{rms}/S \approx 0.25Re_\lambda/(Sq^2/\epsilon_D)$. Assuming that the initial centreline vorticity ω_1 of the hairpins is proportional to ω_{rms} (e.g. $\omega_1 \approx 3\omega_{rms}$, following the comments on p. 45 of RM) and using our previous asymptotic correlation for Sq^2/ϵ_D, we find that $\omega_1 \approx A_5\,5\,Re_\lambda^{\frac{3}{5}}$, where the constant A_5 is between about 0.6 and 1.0. The circulation Γ_0 of the hairpins (which is constant with time) is then given by

$$\Gamma_0 = \pi\sigma_1^2\omega_1 = \pi A_1^2 A_5\,\nu Re_\lambda^{\frac{3}{5}}, \tag{49}$$

where we have used the estimate (45) for σ_1.

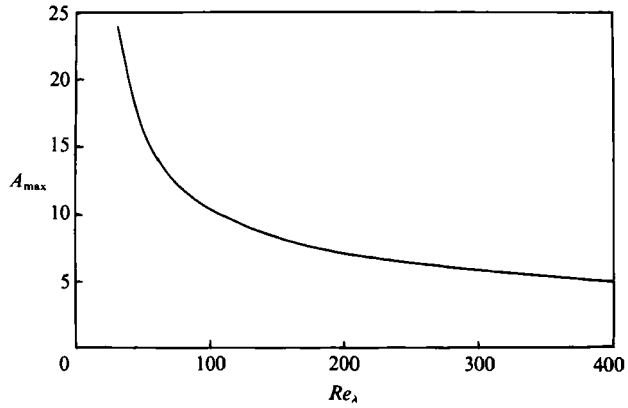

FIGURE 5. Maximum value of the perturbation amplitude ratio A for turbulent hairpin vortices as a function of the microscale Reynolds number Re_λ. The values shown are for the symmetric mode with β_0 adjusted to give the maximum value of A.

(v) The initial vortex length L_I is needed in the stability analysis only to estimate β_{min}. For this purpose, we simply assume that L_I is approximately equal to the mixing length L_M. (Since β_{min} turns out to be smaller than the fastest growing value of β, this assumption does not affect our numerical results.)

With use of the estimates (45)–(49), the four parameters listed in (42) that determine the hairpin stability can be approximated for a hairpin inclination angle θ of 45° as follows:

$$c_1/c_3 = -1, \quad \beta = \beta_0 \exp(-\epsilon\tau), \quad \epsilon = 0.04\, Re_\lambda^{\frac{1}{2}}, \quad \delta = \beta_0 Re_\lambda^{-\frac{3}{8}} \exp(-\tfrac{3}{2}\epsilon\tau). \tag{50}$$

In writing (50), the coefficients A_1 and A_5 in (45) and (49) have been set equal to 7 and 0.8, respectively. Also, using (45)–(49), β_{min} can be approximated as

$$\beta_{min} = 19.8\, Re_\lambda^{-\frac{4}{5}} \exp(-\epsilon\tau). \tag{51}$$

We note that the ratio of core radius σ to leg separation b is given by

$$\sigma/b = 1.6 Re_\lambda^{-\frac{3}{8}} \exp(-\tfrac{1}{2}\epsilon\tau). \tag{52}$$

For $Re_\lambda > 20$, the ratio σ/b is less than 0.5 for all initial times, and σ/b always decreases exponentially as τ increases. Recalling that the cores either touch or overlap when $\sigma/b \geqslant 0.5$, we find that for $Re_\lambda > 20$ the cores will not touch for any τ (except if they are brought together by an instability). These observations rule out the two-dimensional strained vortex instability mechanism of Moore & Saffman (1971) as a primary mechanism for hairpin vortex break-up.

The solution of the system of equations (24) with β, δ, ϵ and c_1/c_3 given by (50) can be used to determine the change in the perturbation amplitude ratio A, defined by (29), as a function of dimensionless time τ for different Re_λ and $\beta_0 \geqslant \beta_{min,0}$. The value of β_0 which gives the greatest perturbation amplitude for a given value of Re_λ is denoted by β_f. For Re_λ between 20 and 400, β_f was found to vary between 3.0 and 1.7. In all runs with $\beta_0 = \beta_f$, the perturbation amplitude ratio A initially increased and then eventually approached a constant value as $\tau \to \infty$, in accord with the comments made following (31). The maximum value of A with $\beta_0 = \beta_f$, denoted by A_{max}, is plotted in figure 5 as a function of Re_λ. Figure 5 shows a decrease in A_{max} as Re_λ increases, which is in accord with the observation (e.g. Head & Bandyopadhyay

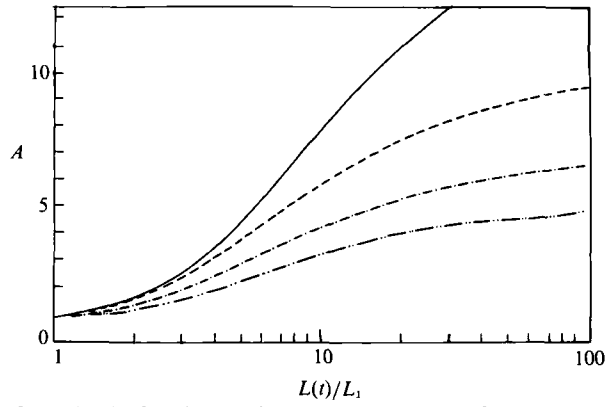

FIGURE 6. Amplitude ratio A of turbulent hairpin vortices as a function of vortex stretch L/L_1 for values of the microscale Reynolds number Re_λ of 50 (——), 100 (– – –), 200 (—·—·—) and 400 (—··—··—). The values shown are for the symmetric mode with β_0 adjusted to give a maximum value for A.

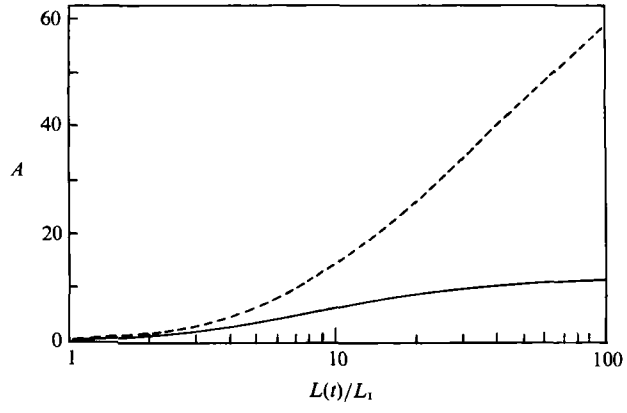

FIGURE 7. Amplitude ratio of turbulent hairpin vortices at $Re_\lambda = 70$ and $\beta_0 = 2.0$ as a function of vortex stretch L/L_1, as calculated both by including the effect of stretching (——) and by neglecting the stretching effect (– – –). The calculations are for the symmetric mode.

1981) that the typical hairpin stretch increases with increasing Reynolds numbers. Of particular note is the rapid increase in $A_{\max}$ as Re_λ is decreased below about 100. The results in figure 5 (and also figures 6 and 7) are for the symmetric mode; antisymmetric disturbances do not grow significantly with time.

The perturbation amplitude ratio A is plotted against vortex stretch $L(t)/L_I$ (again with $\beta_0 = \beta_I$) in figure 6 for four values of Re_λ. At $Re_\lambda = 50$, A becomes fairly large (greater than 10) for a hairpin stretch of only about 15, whereas at $Re_\lambda = 400$, A is never more than 6 no matter how much the hairpin is stretched. These results are significantly affected by the modifications made in §2 to the Crow instability due to the presence of vortex stretching. For instance, in figure 7 a comparison is made between the perturbation amplitude at $Re_\lambda = 70$ and $\beta_0 = 2.0$ as it is calculated with account taken for the effect of axial stretching (solid line), as discussed in §2, and without account being taken for this effect (dashed line). The latter curve is calculated by allowing stretching to change the wavenumber and core radius as

indicated in (49), but not including the effect of stretching in calculating the change in perturbation amplitude (i.e. by neglecting the diagonal terms of the matrix $\boldsymbol{A}_s$ in (22*c*)). Figure 7 clearly shows that axial stretching inhibits the growth of the perturbation. In fact, as $L(t)/L_1 \to \infty$, the prediction in figure 7 that was calculated without accounting for the stretching effect yields unbounded growth of the perturbation, whereas the prediction that includes the stretching effect yields a finite value of A of about 13 in this limit.

The numerical values of the results presented in figures 5–7 are fairly sensitive to the value of the coefficient of ϵ in (50), and hence to the values of the coefficients A_1 and A_5 in (45) and (49). We have selected values for these coefficients which fall within the observed range and have obtained predictions from the stability theory that seem to be qualitatively in accord with observations of hairpins in turbulent shear flows. Variation of these coefficients within their indicated ranges will change the numerical values of our predictions but not our qualitative conclusions.

The maximum perturbation amplitude of a hairpin vortex is obtained by multiplying the initial perturbation amplitude by the value of $A_{\max}$ in figure 5 for the appropriate microscopic Reynolds number Re_λ. Any assessment of maximum hairpin stretch (as a function of Re_λ) in a turbulent shear flow would have to first estimate the initial perturbation amplitude as a function of initial wavenumber. The initial perturbation of the hairpin may be due either to small-scale turbulence or to interactions between two hairpins or between a hairpin and other large vortical structures in the flow.

Before closing this section, it is noted that the local-induction approximation (LIA) of Arms & Hama (1965) is of limited use for calculation of vortex structure evolution in turbulent flows. While calculations based on LIA seem to accurately portray the initial generation and evolution of hairpin vortices (e.g. Aref & Flinchem 1984), LIA is not adequate for calculations of instability and break-up of hairpin vortices. In particular, since mutual induction between opposing legs of a vortex pair is neglected by LIA, calculations which make use of LIA do not exhibit the Crow instability.

Some further comments regarding the interaction between the hairpin core vorticity and the ambient shear vorticity may also be appropriate. It is recalled that in a flow consisting of a streamwise vortex immersed in a shear flow directed along the vortex axis and with no stretching in the x-direction, the transverse shear vorticity and the streamwise vortex vorticity interact to create an expulsion of vorticity from the inner regions of the vortex core (Pearson & Abernathy 1984; Moore 1985). This expulsion occurs on the timescale $(\nu t)^{\frac{1}{2}}$ of viscous diffusion. Although this phenomenon may have some effect on streamwise vortices in turbulent shear layers, it is not believed to significantly influence inclined hairpin vortices. In particular, we note that hairpin vortices are strongly stretched, which acts to counter the viscous diffusion processes responsible for the vorticity expulsion. For example, the Burgers model of a stretched vortex (which has been used by a number of previous investigators as a model for hairpin legs) is initially dominated by vortex stretching and later reaches a final state where stretching and diffusion balance each other. Secondly, in hairpin vortices oriented at some angle θ ($\approx 45°$) to the direction of shear, a shear flow exists exterior to the vortex core, but it is not oriented along the vortex axis. The axial flow interior to the vortex core is mainly due to stretching of the hairpin and is believed to be nearly axisymmetric about the core axis. Further justification for this viewpoint is provided by direct simulations of turbulent hairpin vortices (such as those of RM) which do not exhibit noticeable vorticity expulsion.

4. Conclusions

The problem of the three-dimensional stability of a counter-rotating vortex pair is studied analytically. The problem is reduced to a pair of linear, first-order ordinary differential equations, which can be solved numerically using any standard forward-marching technique. The motion of the vortices (non-dimensionalized by the initial perturbation) is found to depend on four dimensionless constants (ϵ, c_1/c_3, δ_0, β_0), the dimensionless time τ and the ratio of the initial values of the perturbations in the x- and y-directions. It is found that for cases where the stretching rate in the z (axial) direction is greater than zero and where no stretching occurs in the x- or y-directions (so that c_1/c_3 lies between -1 and 0), the perturbation amplitude may initially grow in time (sometimes reaching quite large values) but the perturbations always remain bounded at very large times. For cases in which c_1/c_3 lies in the interval $-1 < c_1/c_3 < 0$, it is found that the perturbations approach zero at infinite time. When c_1/c_3 is equal to either -1 or 0, the perturbations will asymptotically approach a constant amplitude at large times.

The results of the study are applied to an idealized model of a hairpin vortex, which is commonly found in turbulent shear flows. Rough estimates for the various initial geometrical characteristics of the hairpin vortex model (such as leg length and separation distance, vortex circulation, core diameter and stretching rate) are obtained from a recent direct numerical simulation of homogeneous turbulent shear flow. The ratio of the perturbation amplitude at the current time to the initial perturbation amplitude is found to be a function only of the microscale Reynolds number Re_λ of the turbulent flow, the perturbation wavelength and the stretch of the hairpin vortex. In general, this ratio decreases as Re_λ increases, corresponding to the observation that the typical stretch of hairpin vortices in turbulent flows increases as Re_λ increases. Stretching is found to exert a strong stabilizing influence on turbulent hairpin vortices. It is interesting to note, in fact, that in the absence of stretching, many of the hairpin vortices observed in experiments and numerical simulations of turbulent flows are unstable to three-dimensional disturbances and would quickly break up.

REFERENCES

Aref, H. & Flinchem, E. P. 1984 Dynamics of a vortex filament in a shear flow. *J. Fluid Mech.* **148**, 477–497.

Arms, R. J. & Hama, F. R. 1965 Localized-induction concept on a curved vortex and motion of an elliptic vortex ring. *Phys. Fluids* **8**, 553–559.

Burgers, J. M. 1948 A mathematical model illustrating the theory of turbulence. In *Advances in Applied Mechanics* (ed. R. von Mises & T. von Kármán), p. 171. Academic.

Crow, S. C. 1970 Stability theory for a pair of trailing vortices. *AIAA J.* **8**, 2172–2179.

Head, M. R. & Bandyopadhyay, P. 1981 New aspects of turbulent boundary-layer structure. *J. Fluid Mech.* **107**, 297–338.

Kida, S. 1981 Motion of an elliptical vortex in a uniform shear flow. *J. Phys. Soc. Japan* **50**, 3517–3520.

Lundgren, T. S. & Ashurst, W. T. 1989 Area-varying waves on curved vortex tubes with application to vortex breakdown. *J. Fluid Mech.* **200**, 283–307.

Marshall, J. S. 1991 A general theory of curved vortices with circular cross-section and variable core area. *J. Fluid Mech.* **229**, 311–338.

Moin, P. & Kim, J. 1985 The structure of the vorticity field in turbulent channel flow. Part 1. Analysis of instantaneous fields and statistical correlations. *J. Fluid Mech.* **155**, 441–464.

Moore, D. W. 1972 Finite amplitude waves on aircraft trailing vortices. *Aeronaut. Q.* **23**, 307–314.

MOORE, D. W. 1985 The interaction of a diffusing line vortex and an aligned shear flow. *Proc. R. Soc. Lond.* A **399**, 367–375.

MOORE, D. W. & SAFFMAN, P. G. 1971 Structure of a line vortex in an imposed strain. In *Aircraft Wake Turbulence* (ed. J. H. Olsen, A. Goldburg & M. Rogers), pp. 339–353. Plenum.

MOORE, D. W. & SAFFMAN, P. G. 1972 The motion of a vortex filament with axial flow. *Phil. Trans. R. Soc. Lond.* A **272**, 403–429.

MOORE, D. W. & SAFFMAN, P. G. 1975*a* The density of organized vortices in a turbulent mixing layer. *J. Fluid Mech.* **69**, 465–473.

MOORE, D. W. & SAFFMAN, P. G. 1975*b* The instability of a straight vortex filament in a strain field. *Proc. R. Soc. Lond.* A **346**, 413–425.

NEU, J. C. 1984 The dynamics of a columnar vortex in an imposed strain. *Phys. Fluids* **27**, 2397–2402.

PEARSON, C. F. & ABERNATHY, F. H. 1984 Evolution of the flow field associated with a streamwise diffusing vortex. *J. Fluid Mech.* **146**, 271–283.

PIERREHUMBERT, R. T. & WIDNALL, S. E. 1981 The structure of organized vortices in a free shear layer. *J. Fluid Mech.* **102**, 301–313.

ROBINSON, A. C. & SAFFMAN, P. G. 1982 Three-dimensional stability of vortex arrays. *J. Fluid Mech.* **125**, 411–427.

ROBINSON, A. C. & SAFFMAN, P. G. 1984 Three-dimensional stability of an elliptical vortex in a straining flow. *J. Fluid Mech.* **142**, 451–466.

ROGERS, M. M. & MOIN, P. 1987 The structure of the vorticity field in homogeneous turbulent flows. *J. Fluid Mech.* **176**, 33–66 (referred to herein as RM).

ROSENHEAD, L. 1930 The spread of vorticity in the wake behind a cylinder. *Proc. R. Soc. Lond.* A **127**, 590–612.

WIDNALL, S. F. & BLISS, D. B. 1971 Slender-body analysis of the motion and stability of a vortex filament containing an axial flow. *J. Fluid Mech.* **50**, 335–353.